# 3. Geophysical Fluid Dynamics

**Experimental study on the three dimensional spherical convections with the parameters of planetary atmospheres**


Contact Person: Yoshi-Yuki Hayashi

Department of Earth and Planetary Physics

University of Tokyo[1]

Research Organization: Yoshihisa Matsuda, Yoshi-Yuki Hayashi, Shin-ichi Takehiro[2]

Masaki Ishiwatari, Masahiro Hosaka[3]

Geophysical Fluid Dynamics group, Division of Meteorology

Department of Earth and Planetary Physics, University of Tokyo



Keywords: spherical convection, general circulation, planetary atmospheres, angular momentum, zonal mean flow, teleconnection patterns, SST anomaly, heating response


## 1. Background

The grand purpose of our study is to reveal the dynamical structures which underlie the general circulations of the planetary atmospheres. It is aimed to construct a theoretical framework which is useful in describing their circulation characteristics, as tried by Golitsyn[1] since 1960's $\sim$. Our interest in due course is to recognize the atmosphere of the earth (or the climate of the earth) as one of the possible realizations in the physical parameter space observed in the solar system.

One of our procedures in revealing the possible underlying dynamics is to gather and classify atmospheric circulation patterns which might be observed under various values of planetary "external" conditions such as orbital parameters (amount and variation of the incoming solar flux), radius and rotation rate of the planet, radiation property of the atmosphere, and surface boundary setups. The sampling of the possible atmospheric circulations is partly possible by numerical experiments by the use of the super computer powers.

Our search in circulation patterns is now performed for the following three major targets:

1. to reveal the possible circulations which might be realized with the earth's condition, but with strongly simplified surface and/or physical processes,
2. to reveal the possible circulations which might be realized with the values of solar flux and orbital parameters which are related to Mars, Earth and Venus,
3. to reveal the possible circulations which might be realized as convection of a spherical shell in general.

These are the targets being studied continuously from the preceding years.

The first target includes so called aqua-planet experiment, where all the surface is assumed to be covered by the ocean[2-4]. The aim is to answer the basic problem of the climate, that is, "where and how does it rain?". In the aqua-planet experiments performed so far, the focus has been placed on especially in searching for the idealistic precipitation distribution of the tropics. The experiment performed here is also in this category, however, the new feature is to find out the deformation of the precipitation distribution to a warm SST (sea surface temperature) anomaly placed in the tropics. The configuration is supposed to extract the effect of the warm SST region in the real Western Pacific on the general circulation patterns.

The second target is the three dimensional calculations of the so called runaway greenhouse effect. It has been argued, in relation to the evolution of the atmospheres of Venus, Earth and Mars, that there exists a limit of radiation which can be emitted from the top of the atmosphere with the ocean[5]. The interesting point is that the radiation limit predicted in the literature is not far from the value of the incoming solar flux of the present earth. It is about 300 W/m$^2$. The argument placed so far is presented by the use of one dimensional models. It is of interest to observe with three dimensional model to what extent the climate of present earth is stable to the variation of the solar constant. The present concern is to assess the calculation possibility of the evaporation or the freezing of the oceans.

The third target is to refine the dynamical framework of the rotating spherical convection theory, and also to acquire the description ability of the circulation patterns of the deep "atmospheres" as those of outer planets and the sun. The theory of convection in rotating spherical shells has been intensely considered by Busse and his colleagues[6]. The difficulty in their work is that the description utilized is too much mathematical, and hence it is not easy to acquire physical insight. Especially for the distribution of the angular momentum, there has not been presented any satisfactory mechanistic description.

## 2. Aqua planet experiments with SST anomaly

### 2.1 Experimental design

The model utilized is basically the same as that

[1] Present affiliation: Graduate school of Earth Environmental Science, Hokkaidou University

[2] Present affiliation: Oceanography Division, Japan Meteorological Agency

[3] Present affiliation: Numerical Prediction Division, Japan Meteorlogical Agency

used in [3]. It is the code originally produced by Dr. Numaguti of NIES, and is the version now archived and maintained by GFD DENNOU CLUB. The model consists of the three dimensional hydrostatic system on a sphere with very crude physical processes. The dynamical part is represented by the pseudo spectral method with the triangular truncation at wavenumber 42 (T42) and 16 vertical levels. The cumulus parameterizations are Kuo or adjustment scheme. The vertical diffusion is represented by Yamada-Meller Level II scheme. The surface fluxes are evaluated by the usual bulk formula. The radiation processes include four bands, which are very roughly tuned to give the mean temperature structure resembling the real atmosphere.

The surface is all covered by the ocean (aqua-planet). Note that in the experiments described in this section the value of SST is fixed. The SST distribution for the control experiment is zonally uniform and symmetric about the equator, and has its peak value at the equator. The peak amplitude is 301.2K, which is the same as that of Numaguti's experiments[4].

The shape of anomalous SST placed at the equator has been changed from the experiments performed last year. It is now of a gaussian distribution with e-folding scales of 10° latitudinally and 20° longitudinally. There are three experiments depending on the placed peak values of the anomalous SST; 3K, 5K, and 7K.

The reason for changing the SST shape is that the former experiments did not yield a precipitation distribution which has a single peak. The SST distribution was formerly of an elliptical area with diameters of 60° in the longitudinal direction and 20° in the latitudinal direction. The amount of SST was increased by +2K uniformly. This SST shape caused double peaks at near the both longitudinal edges of the anomalous region, which itself is of interest, but gives some difficulty in the dynamical interpretation of the resulting circulation feature, since the atmospheric waves generated by the two intensive precipitation (diabatic heating) interfere to each other, and consequently the possible remote response becomes dynamically obscure.

Please note that in this new experiment series the intensity of anomalous SST is increased by unrealistically large. This is to figure out possible underlying characters by investigating artificial unusual cases.

2.2 Results

Figure 1 shows the 300 day averaged precipitation patterns obtained by the anomalous SST with a peak value of +3K. Note that the unit of the values in the figure is W/m$^2$. As previously reported, it is obviously observed that precipitation is substantially suppressed for about 30° longitudinal width in the west of the SST anomaly. In the east of the anomaly, the double ITCZ structure remains almost as it is under the control condition (no anomalous SST case, not shown). This result contrasts with the results of previous experiments with a +2K flat SST anomaly, where the double ITCZ structure was destroyed; the precipitation peak tends to appear at the equator.

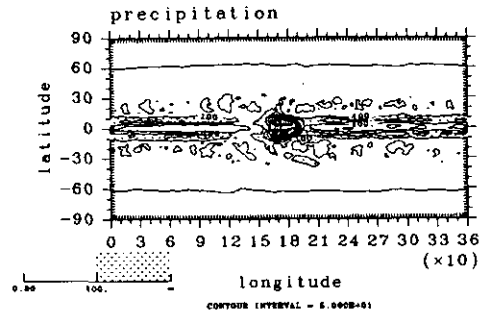


Figure 1

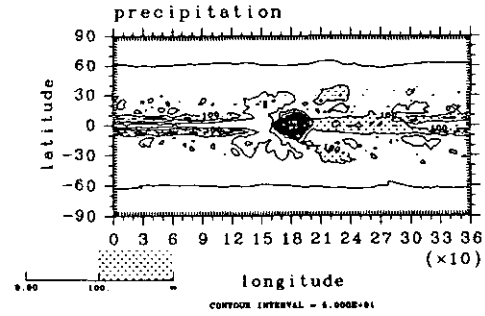


Figure 2

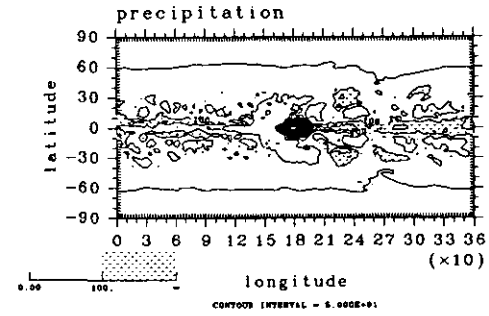


Figure 3

Figure 2 shows the 300 day precipitation patterns obtained by the anomalous SST with a peak value of +5K. Now, the double ITCZ structure in the east of the SST anomaly is destroyed. The precipitation peak tends to appear at the equator. In the subtropical regions, the amount of precipitation decreases in the west of the anomaly, while it is increased in the east of the anomaly. These are the features obtained in the former experiments with a +2K flat SST anomaly. The rea-

son why those features are recovered for +5K anomaly is considered that the amount of precipitation, i.e., diabatic heating reaches comparable amount to that of former +2K flat SST anomaly.

Figure 3 shows the 300 day precipitation patterns obtained by the even more extraordinary SST anomaly of a peak value of +7K. The single ITCZ area to the east of the SST anomaly extends to the other hemisphere (to the west of the SST anomaly).

To what extent the given SST anomaly alters precipitation pattern seems to depend not only on equatorial wave dynamics but on the intensity of realized precipitation anomaly at the equator, which should be understood by considering thermodynamic constraints. Figure 4 shows the precipitation profiles at the equator of those three experiments. As the intensity of SST anomaly increases, the amount of precipitation at the anomalous region naturally increases. The interesting thing to note is that the amount of precipitation to the west of anomaly is minimum for +3K anomaly; it increases gradually with increasing SST anomaly. This probably is due to the eastward propagating waves generated at the SST anomalous region. The wave amplitude becomes larger as the increased precipitation anomaly at the SST anomalous region, and eventually overcomes the drying effect to the west of the SST anomaly.

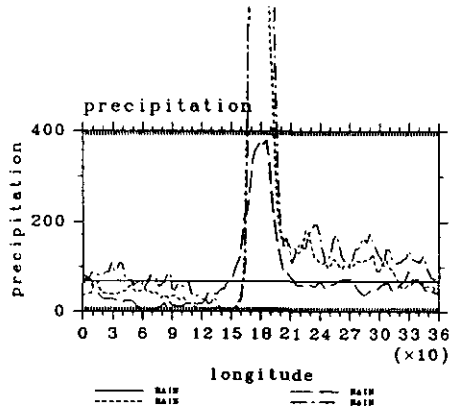


Figure 4

3. Aqua planet experiments for runaway greenhouse condition

3.1 Experimental design

The model utilized is basically the same as that used in the previous section. It is the three dimensional hydrostatic system on a sphere with very crude physical processes. The dynamical part is represented by the pseud spectral method with the triangular truncation at wavenumber 21 (T21) and 16 vertical levels. Note that the horizontal resolution is reduced in order to integrate for the longer period in order to trace the evolution of the thermal structure. The vertical diffusion and the surface fluxes are evaluated by the same scheme as the previous section.

The radiation processes utilized is the exactly same thing as that of [5]. There is no scattering. Only the water vapor absorb the long wave radiation and the absorption coefficient is gray. The sun is assumed to be at the equinox position. hence the zonal mean incoming solar flux is symmetric at the equator.

The surface is all covered by the ocean (aqua-planet). But in this section, the SST is not fixed. The surface does not have heat capacity. The radiation flux, sensible flux, and latent flux are in balance at the surface at any time. This is the so called swamp condition.

The experiments performed this year focuses on the comparison of the effect of cumulus parameterizations on the appearance and the structure of the runaway greenhouse states. In the preceding year, the utilized cumulus parameterization was so called large scale condensation only. This is because we do not have almost any knowledge on the form of precipitation around the runaway greenhouse situation. We just decide to use the simplest one. It was confirmed that the model really gave the runaway greenhouse state, after integration for 500 days.

The utilized cumulus parameterizations are 1) only large scale condensation (same as that of previously reported), 2) adjustment scheme, 3) Kuo scheme. The solar constant is fixed to be 1800 $W/m^2$, i.e., the averaged solar flux is 450 $W/m^2$. This is the value the existence of the runway greenhouse was confirmed previously. The integration period is 500 days as before.

3.2 Dependency on cumulus parameterization.

The evolutions of the global mean temperature and OLR (outgoing longwave radiation) do not differ very greatly between the results of different cumulus parameterization. All of the utilized parameterization scheme resulted in sufficiently wet atmosphere, which reduced the atmospheric long wave emission to the space. The value of global mean emission is about 400 $W/m^2$, which is well below the input solar flux, 450 $W/m^2$. The atmosphere is going runaway.

Although the global heat budget becomes similar to each other, some difference can be found in the latitudinal thermal budget. Figure 5, 6 and 7 are the latitudinal thermal budget profiles for large scale condensation only, adjustment parameterization, Kuo parameterization, respectively. In the case of large scale condensation only, the precipitation intensity is largest at the polar region (Figure 5), while in the cases of adjustment and Kuo parameterization it is the largest at the equator. The reason why we have such a distribu-

tion is now being investigated.

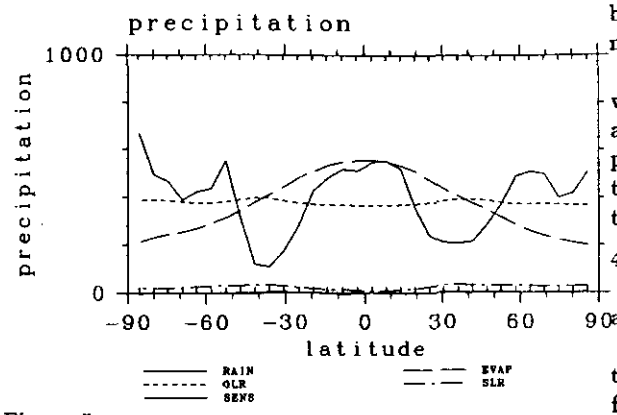


Figure 5

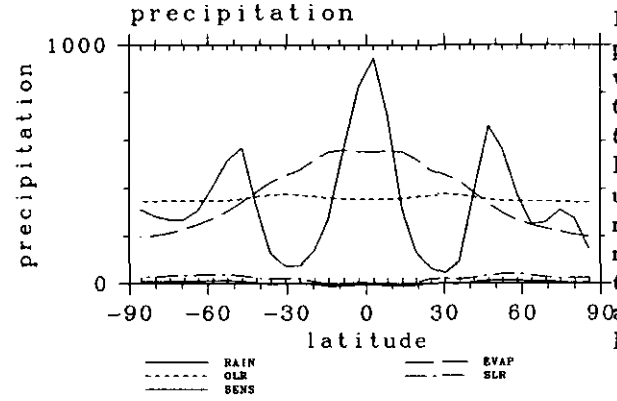


Figure 6

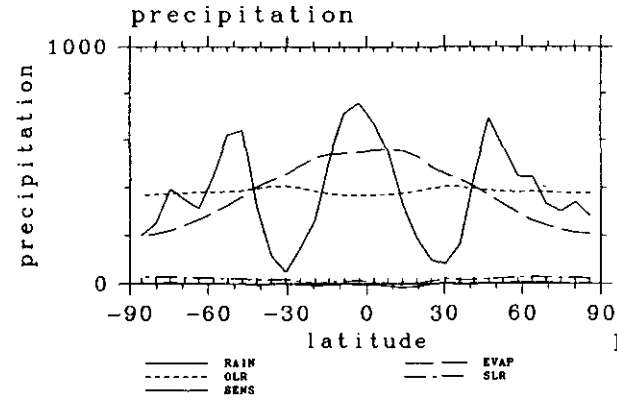


Figure 7

4. Boussinesq convection in a spherical rotating shell.

4.1 Experimental design

In order to reinforce the knowledge of formation of zonal mean flows, we start from a reconsideration of the zonal mean flow distributions induced by Boussinesq convection in a spherical rotating shell. This is the typical starting point of the thorough theoretical consideration. To start with the consideration is limited to the cases where rotation rate is small. The conditions considered include homogeneous internal heat sources and fixed temperature boundaries as the thermal conditions, and free-slip boundaries as the kinematic conditions. This is a standard set of boundary conditions in the sense that many investigations have been performed already. However, the classification of momentum redistribution is not considered so far.

The calculation performed here just follows the weak nonlinear procedure. The linear critical modes are numerically calculated by solving the linear stability problem. Then the zonal mean flows which equilibrate the acceleration due to the nonlinear forcing caused by the linear critical modes are also numerically calculated.

4.2 Zonal mean flow acceleration

The calculated distribution of mean zonal flows are shown in Figure 8 and 9.

Figure 8 is the result for the cases of low rotation rate, i.e., Taylor number $Ta = 10$. Figure 8a is for the case where the ratio of the inner radius to the outer radius is $\eta = 0.6$ and Prandtle number is $Pr = 1$. Note that the westerly (super rotating) region appears at the equatorial region. Figure 8b is for the case where $\eta$ is unchanged but Prandtle number is increased to $Pr = 100$. Note that the easterly region appears at the equatorial region. Figure 8c is for the case where Prandtle number is the same as that presented in Figure 8a but the ratio of the inner radius to the outer radius is decreased to $\eta = 0.4$. Note that the easterly region appears again at the equatorial region. When the layer depth is large, the induced zonal mean flows at the equator is alway easterly. It does not depend on Prandtle number.

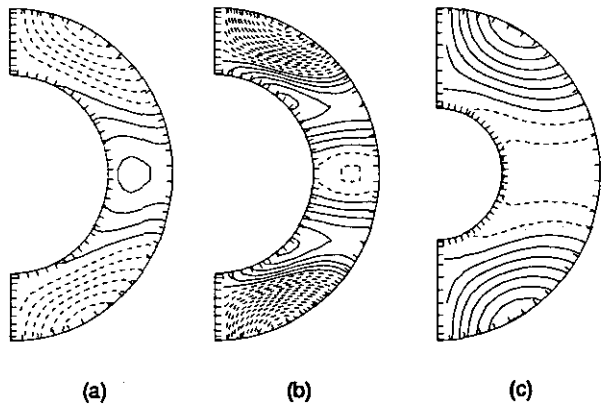


Figure 8

Figure 9 is the result for the cases of high rotation rate, i.e., Taylor number $Ta = 10^6$ . Figure 9a is for the case where the ratio of the inner radius to the outer radius is $\eta = 0.4$ and Prandtle number is $Pr = 1$. Note that the westerly (super rotating) region appears at the equatorial region. Figure 9b is for the case where $\eta$ is unchanged but Prandtle number is increased to $Pr = 100$. Note that the easterly region appears at the equatorial region. Figure 9c is for the case where Prandtle number is the same as that presented in Figure 9a but the ratio of the inner radius to the outer radius is increased to $\eta = 0.8$. Note that when the rotation rate is high there appears no thickness dependency of

the direction of the zonal mean flow.

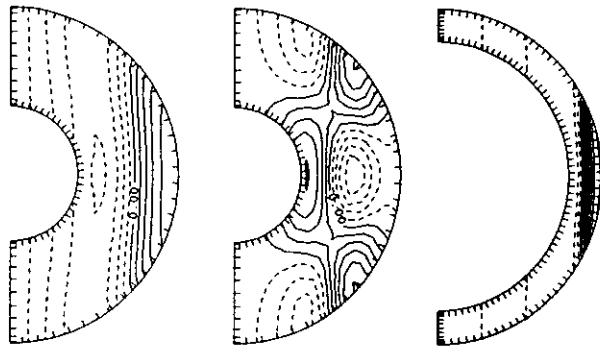

(a) (b) (c)

Figure 9

Those tendency should be understood by the variation of relative importance of the transports of angular momentum between by mean meridional circulations $\langle \Omega \overline{v} r \cos^2 \phi \rangle$ and by Reynolds stresses $\langle \overline{uv} \cos \phi \rangle$. The total angular momentum transport is described by

$$\frac{\partial}{\partial t} \langle \overline{u} r \cos \phi \rangle + \frac{1}{\cos \phi} \frac{\partial}{\partial \phi} \left[ \cos \phi \left( \langle \Omega \overline{v} r \cos^2 \phi \rangle + \langle \overline{uv} \cos \phi \rangle \right) \right] = \langle F_\lambda r \cos \phi \rangle,$$

where $r$ is radius, $\phi$ is longitude, $u$, $v$ is eastward and northward wind, $\langle\rangle$ is vertical mean, $\overline{()}$ is zonal mean, $F_\lambda$ is frictional diffusion term.

The Reynolds stress due to convective cell causes westerly acceleration, because $\overline{uv}$ becomes equatorward owing to the Coriolis effect. The structures of the linear disturbances are different between the cases of high rotation rates and low rotation rates. When the rotation rate is high, the disturbances have Rossby wave structure, while when the rotation rate is low, the disturbances have more like the shape of simple direct convective cells. However they happen to yield the same sing for $\overline{uv}$.

Another effect is the mean meridional circulation. Since the mean meridional circulation is from equator to pole in the outer region while pole to equator in the lower region, the mean transfer of angular momentum due to mean meridional circulation causes easterly acceleration.

Now, consider when Prandtle number is large, that is, friction is increased. The velocity correlation due to Coriolis effect becomes small and thus easterly acceleration occurs.

Similarly, when the radius of the inner sphere is small, the mean meridional circulation transport the momentum to the higher latitudes more efficiently, and again, eastward acceleration occurs. However, this is not realized in the calculations presented here. In the case of Figure 8c where easterly flow is obtained at the equator, the acceleration itself is westerly. The realized flow has the opposite sign to that of acceleration. This is due to the inertial effect of the rotating sphere. When the rotation rate is high, the structure of the linear disturbance is changed and this inertial effect does not appear any longer.

Acknowledgement

We wish to thank Drs. Mitsumoto, Numaguti, and other NIES staff members for providing us with this powerful computing facility. A number of suggestions and supports by Dr. Numaguti on softwares, hardware usages, and sciences were indispensable to our research performance. Our software environment was provided from the resources of GFD DENNOU CLUB. GFD DENNOU CLUB is an independent group of scientists aiming at collecting basic software resources for research and education of geophysical fluid dynamics and related fields. Those resources include three dimensional spherical primitive system originally developed by Dr. Numaguti while he was at University of Tokyo. We also have to express our thanks to the staffs of TISN (Tokyo university International Science Network) in providing us with data connection between NIES and University of Tokyo.

References

1. G.S. Golitsyn, *ICARUS*, **13**, 1 (1970)
2. Y.-Y. Hayashi and A. Sumi, *J. Met. Soc. Japan*, 64, 451 (1986)
3. A. Numaguti and Y.-Y. Hayashi, *J. Met. Soc. Japan*, 69, 541 (1991)
4. A. Numaguti, *J. Atmos. Sci.*, **50**, 1874 (1993)
5. S. Nakajima, Y.-Y. Hayashi and Y. Abe, *J. Atmos. Sci.*, 49, 2256 (1992)
6. K.-K. Zhang and F.H. Busse, *Geophys. Astrophys. Fluid Dynamics.*, 39, 119 (1987)

# Direct Numerical Simulation of Liquid Mixing Layer with Second-Order Chemical Reactions


Contact Person — Associate Professor, Satoru Komori
Dept. of Chemical Engineering, Kyushu University

(Research Organization) — PhD Student, Ryuichi Nagaosa
Dept. of Chemical Engineering, Kyushu University

MC Student, Ryoichi Kurose
Dept. of Chemical Engineering, Kyushu University

Section Head, Shunji Takeshita
National Institute for Environmental Studies,
Environmental Agency of Japan

Senior Scientist, Kunio Kohata
National Institute for Environmental Studies,
Environmental Agency of Japan



*Keywords* — atmospheric diffusion, oceanic diffusion, chemical reaction, turbulent mixing, DNS, reactive-diffusive mechanism


## 1. Introduction

When two reactants are introducted into a turbulent flow, turbulent mixing plays an important role on the progress of the chemical reaction until two species are perfectly mixed up to the minimum scale of turbulence. The effect of turbulent mixing on the reaction rate is very significant for higher-order reactions, which often appear in enviromental flows or industrical reactors. It is, therefore, of great importance to investigate the reactive difusive mechanism in both estimating the turbulent diffusion of reactive contaminants in the atmosphere and oceans and designing industrial combustors and reactors.

One of good ways for studying the reactive-diffusive mechanism in a reacting flow is to solve numerically continuity, Navier-Stokes(NS) and mass transport equations without closure assumptions. We consider a second-order, irreversible and isothermal reaction:

$$A + B \rightarrow P. \tag{1}$$

The continuity, NS and mass transport equations for a second-order reaction between reactive species A and B are given by

$$\frac{\partial U_i}{\partial x_i} = 0 \tag{2}$$

$$\frac{\partial U_i}{\partial t} + U_j \frac{\partial U_i}{\partial x_j} = -\frac{1}{\rho}\frac{\partial P}{\partial x_i} + \nu \frac{\partial^2 U_i}{\partial x_j^2} \tag{3}$$

$$\frac{\partial C_A}{\partial t} + U_i \frac{\partial C_A}{\partial x_i} = \kappa_A \frac{\partial^2 C_A}{\partial x_i^2} - k C_A C_B \tag{4}$$

$$\frac{\partial C_B}{\partial t} + U_i \frac{\partial C_B}{\partial x_i} = \kappa_B \frac{\partial^2 C_B}{\partial x_i^2} - k C_A C_B \tag{5}$$

However, it is very difficult to carry out the numerical simulation (DNS) for a reacting liquid flow with high Reynolds and Schmidt numbers, since the minimum scale of the concentration fluctuation, i.e., Batchelor scale, is quite small compared to the Kolmogorov scale. To carry out the DNS, huge numerical grid-points are required. Thus, the previous DNS has been limited to reacting gas flow with low Schmidt numbers (e.g., Elghobashi and Nomura[1]), and all direct numerical simurations have been done for homogeneous reacting flows by using a pseudospectral method. However, practical reacting flows in the ocean or chemical reactors often have chemical reactions in the liquid phase and complicated flow configurations. Furthermore, most previous direct numerical simulations in reacting gas flows discuss the reactive-diffusive mechanism under the assumption that the calculations by the DNS have sufficient accuracy, and the predictions have not been compared

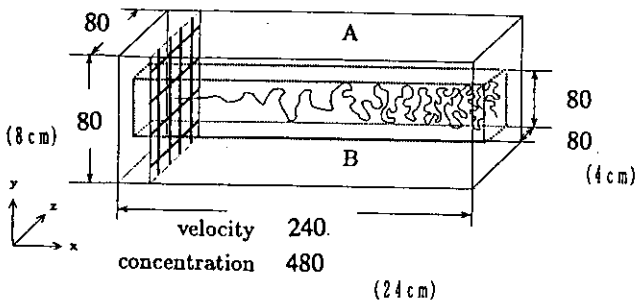


*Fig.1 Sketch of reacting liquid mixing layer behind turbulence grids for DNS.*

with the measurements of concentration statistics because of the lack of the measurements. However, it should be noted that the discussion of the DNS whithout comparisons with the measurements is rather dangerous for reacting flows where two reactive fluids form the sharp interface.

The purpose of our study is, therefore, to solve Eqs.(2)-(5) numerically and clarify the reactive-diffusive mechanism in a reacting liquid flow. As the first stage to achive this purpose, here the reliability of the present DNS was investigated comparing the prediction of velocity and concentration statistics with the measurements of Komori et al.[3),4)].

## 2. Direct Numerical Simulation (DNS)

The geometry of computational region is shown in Figure 1. The three-dimentional DNS was applied to reacting liquid mixing layer behind a turbulence grid by adjusting the boundary conditions to the practical flow geometry. The NS and mass transport equations were transformed into the generalized equations and discretized to construct the finite-difference formulation. The nonlinear terms appeared in the NS equation (Eq.(3)) were approximated by a fifth-order upwind scheme and other spatial derivatives were approximated by a fourth-order central difference. HSMAC method was used here to solve the NS equation(Eq.(3)). The Reynolds number based on the mesh size $M$ was 5000. The streamwise, vertical and spanwise sizes (grid points) of the computational domain were $-1 \leq x/M \leq 11$ and $-2 \leq y, z/M \leq 2$ ($240 \times 80 \times 80$ grid points) for the velocity field, and $-1 \leq x/M \leq 11$ and $-1 \leq y, z/M \leq 1$ ($480 \times 80 \times 80$ grid points) for the concentration

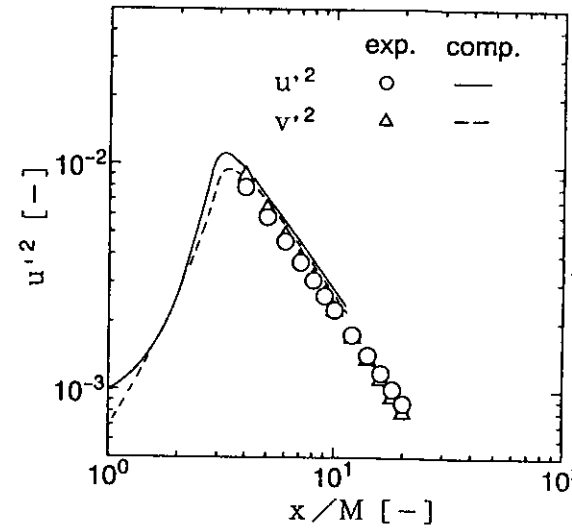


*Fig.2 Decay of velocity fluctuations downstream of the grids.*

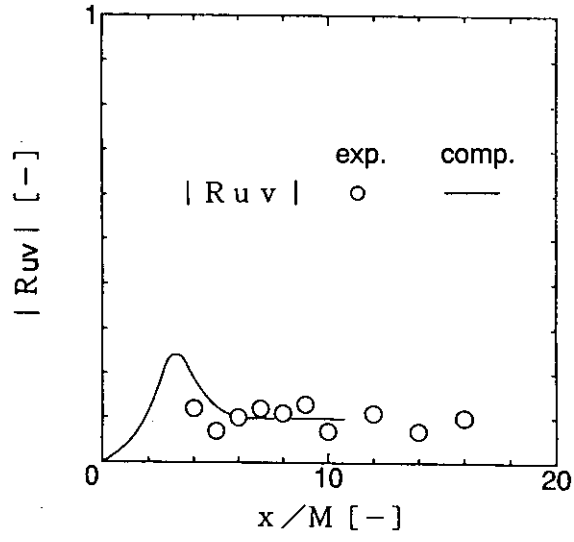


*Fig.3 Longitudinal profiles of the correlation coefficient between velocity fluctuations of u and v.*

field. Therefore, the grid spacing for concentration was the half size of that for velocity. The computations were carried out for three reactions; no reaction, moderately fast reaction and fast reaction.

## 3. Results and Discussion

The decay of u'and v' downstream of the grid is shown in Figure 2. Figure 3 shows the longitudinal profile of the correlation coefficient between two velocity fluctuations, u and v. The decay of the squared turbulence intensities is proportional


*(a) Moderately fast reaction.*


*(b) Fast reaction.*

*Fig.4 Distributions of the countour of instantaneous concentration of product P.*

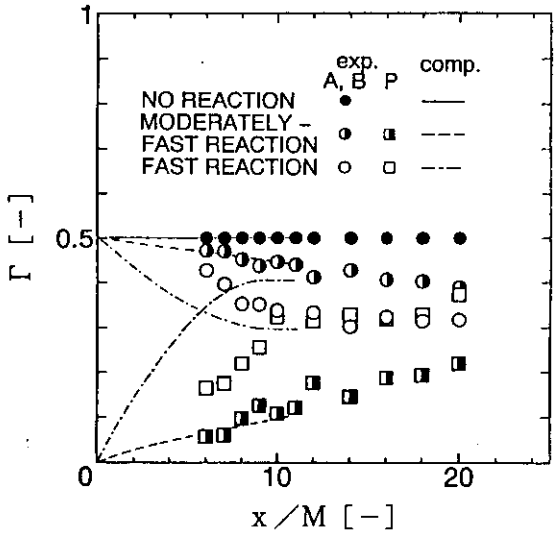


*Fig.5 Longitudinal profiles of mean concentrations of species A and P.*

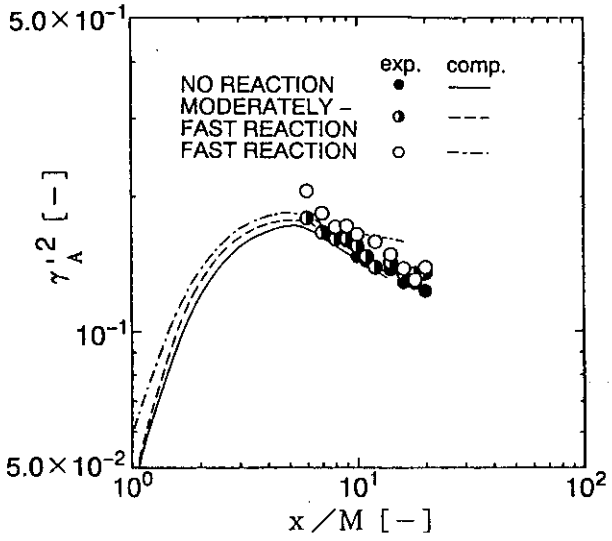


*Fig.6 Longitudinal profiles of the intensities of concentration fluctuations of species A.*

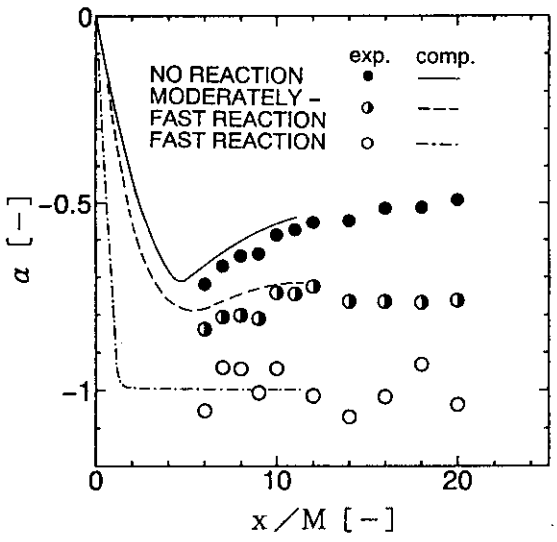


*Fig.7 Longitudinal profiles of the segregation parameter.*

to $(x/M)^{-1.4}$ and agree with the measurements[3),4)]. The correlation coefficient is almost equal to 0.1 for $x/M \geq 4$. These results mean that the flow calculated by the present DNS is an ideal decaying isotropic turbulent flow in the region of $x/M \geq 4$.

Figures 4(a) and (b) show the contour of the concentration of the chemical product in the reacting interfacial region. The thickness of the product in case of a fast reaction is thicker than in case of a moderately fast reaction.

Figures 5, 6 and 7 show the comparisons of the normalized mean concentrations of species A and chemical product P, the intensities of concentration fluctuation and the segregation parameter,

$$\alpha = \frac{\overline{\gamma_A \gamma_B}}{\overline{\Gamma}_A \overline{\Gamma}_B}, \tag{6}$$

with the measurements[3),4)] in a shear-free liquid mixing layer behind the turbulence grids. The predicted turbulence quantities almost agree with the measurements[3),4)] and the agreement exhibits the reliability of the present DNS for a high Schmidt number. However, the predicted mean concentrations of species P in the case of fast reaction (Figure 5) is much larger than the measurement. The mean concentration of species P by the DNS is

over-estimated because the thickness of the interface is thinner than the computational grid spacing and the interface stays near on the center in the early region.

## 4. Conclusions

The DNS was applied to reacting liquid mixing layer behind turbulence-generation grids and the reliability was studied by comparing the measurements[3),4)]. The results show that the present DNS is approximately applicable to reacting flows even in liquid phase.


## Acknowledgements

The computation was carried out by the super computer SX-3 of Central for Grobal Environmental Research, National Institute for Environmental Studies.


## References


1)S.Elghobashi et al., *Turbulent Shear Flow*, **7**, 313 (1991).

2)S.Komori et al., *Phys. Fluids A*, **5**, 115 (1993).

3)S.Komori et al., *Phys. Fluids A*, **3**, 507 (1991).

4)S.Komori et al., *J. Fluid Mech.*, **228**, 629 (1991).